Desalination and Water Treatment
www.deswater.com

doi: 10.5004/dwt.2017.20360

77 (2017) 355–365
May

Comparative studies on removal of methyl orange and sunset yellow dyes using ZnS:Cu–NPs–AC: optimization, equilibrium, kinetic and thermodynamic studies

Hanieh Askari, Mehrorang Ghaedi*, Kheibar Dashtian

Chemistry Department, Yasouj University, Yasouj 75918-74831, Iran, Tel./Fax: +98 74 33223048;
emails: m_ghaedi@mail.yu.ac.ir (M. Ghaedi), askari.hanieh@gmail.com (H. Askari), dashtiankheibar@gmail.com (K. Dashtian)

Received 18 July 2016; Accepted 15 November 2016

ABSTRACT

Copper- doping zinc sulfide nanoparticles (ZnS:Cu–NPs) were synthesized and subsequently in the presence of ultrasound waves were immobilized on activated carbon (ZnS:Cu–NPs–AC). This nanocomposite was characterized by scanning electron microscopy and X-ray diffraction techniques. This material was used for ultrasound-assisted adsorption of methyl orange (MO) and sunset yellow (SY) dyes in single solution, and obtained results were compared with each other. It has been demonstrated that the removal percentage can be improved by the combination of ultrasonication and adsorption processes. The best pH searched via one factor-at-a-time method was found to be 5.0 for each dye. Subsequently, initial concentration of dyes (mg L^{-1}), amount of ZnS:Cu–NPs–AC (g) and sonication time (min) influence on dyes' removal percentage were studied by central composite design combined with desirability function. Desirability scores of 0.9086 and 0.9441 correspond to maximum removal percentage of 97.37% and 86.54% was found for MO and SY respectively. These predictive models were attained at 6.64 and 12 mg L^{-1} of MO and SY concentration, 0.018 and 0.029 g of ZnS:Cu–AC and 4.0 and 4.5 min of sonication time for MO and SY, respectively. The adsorption rate well fitted by pseudo-second order for two dyes, while adsorption capacity according to the Langmuir model as best equilibrium isotherm for MO and SY was found to be 44.65 and 50.54 mg g^{-1}, respectively. The comparison of obtained results shows that ZnS:Cu–NPs–AC has better performance for SY toward MO adsorption.

Keywords: Methyl orange; Sunset yellow; Copper-doping zinc sulfide nanoparticles; Activated carbon; Desirability function

1. Introduction

Methyl orange (MO) and sunset yellow (SY) (Fig. 1) as anionic acid–base indicator or food additive may be toxic and/or carcinogenic agents with similar dye resource [1–6]. Problems in breathing, vomiting, diarrhea, nausea and teratogenic effects are types of their subsequent hazards that make emphasis to researchers for their rapid, cheap and efficient removal and elimination. Treatment techniques are divided into coagulation, adsorption, precipitation, ozonation and biosorption with limitations such as large amount of supporting material and generation of large amount of secondary waste [7–11]. The adsorption as old popular technique need more modifications to be efficient for such purpose [12–14]. Search and design of novel nontoxic, low cost and easily available nanostructure-based adsorbent lead to great improvement in adsorption efficiency. Intermixing carbon-based materials such as activated carbon (AC) with reactive centers like OH, COOH, NH_2 and amide groups with metallic nanocomposites leads to extension in mechanism through π–π, hydrogen bonding, and charged electrostatic force depend on pH [15]. Such favorable modification by improving physicochemical properties (smaller size, intraparticle interaction affinity, high specific surface area and better adsorption capacity) leads to acheivment of high removal percentage and actual amount of adsorption in short

* Corresponding author.

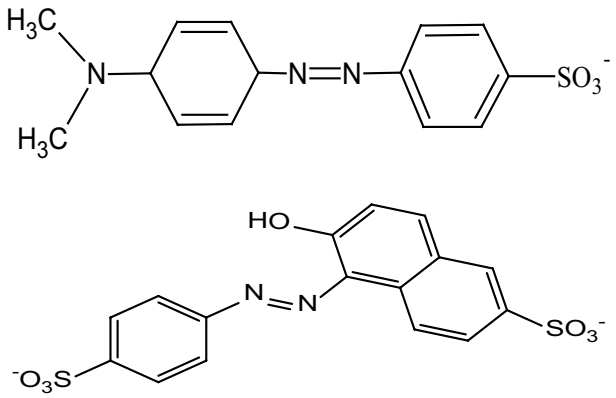

Fig. 1. Chemical structure of MO (a) and SY (b).

time via using small amount of adsorbents. Therefore, nanoparticles eagerly like to loaded AC surface through functional groups, non-localized Π-electron through ion dipole interaction, while presence of its oxygen reactive center also favor loading process through hydrogen bonding via hard–hard interaction. In this case, metallic nanoparticles such as copper and zinc have great importance. Therefore, it seems and expectable that hybrid of AC with metallic NPs has greater and favorable reactive sites toward AC and/or NPs as sole adsorbent. Probable back distribution of such NPs (ions and atoms) may be suitable for living things because of their high threshold limit, while on the other hand such nanoscale material also found to be good anti-bacterial and anti-fungal activities [16–18]. Therefore, copper-doping zinc sulfide nanoparticles loaded on AC (ZnS–Cu–NP–AC) are characterized by X-ray diffraction (XRD) and scanning electron microscopy (SEM) and applied for the ultrasound-assisted adsorption of MO and SY dyes from aqueous media. Recently, to improve the limitations of other processes, such as high cost, ineffectiveness for the removal of pollutants, operation problems and production of toxic secondary contaminations, adsorption combined with other processes for many applications has been accepted as an effective purification process to reduce the organic and inorganic pollutants [19]. One of the innovative technologies used in combination of adsorption is ultrasonic waves. In addition, it has been demonstrated that the removal percentage can be improved by the combination of ultrasonication and adsorption processes due to the disadvantages of them alone such as high cost, ineffectiveness for the adsorption of toxic pollutants, operation problems and production of toxic secondary pollutants [20]. Ultrasound has been proven to exhibit several effects in solid–liquid systems such as the enhancement of mass transfer rate, the increase of the surface area by forming many micro-cracks on the solid surface and the cleanup of solid particle surfaces [21]. The role of ultrasound on the adsorption processes has been recently studied, and controversial effects have been found. Ultrasound waves improved the mass transfer coefficient through cavitation and acoustic streaming, which could be the reason for the enhancement of the adsorption kinetics. The shear forces generated during the cavitation are mostly responsible for the enhancement of MO and SY removal by saffron corm in the presence of ultrasound waves [22].

The effects of operational variables such as initial dyes concentration (mg L^{-1}), ZnS–Cu–NP–AC mass (g) and sonication time (min) on the removal of MO and SY were studied using central composite design (CCD) under response surface methodology. CCD under design of experiments has been used for planning, analyzing and running experiments, which helps to minimize cost and time [23–26]. Also, it enables efficient data collection and reduces error by excluding non-significant factors from the experiment, as well as increasing the accuracy of the results to the target range [27,28].

2. Experimental setup

2.1. Materials and instruments

Chemical reagents including $Cu(CH_3COO)_2$, zinc acetate, thiourea, AC, HCl and sodium hydroxide (NaOH) without further purification were purchased from Merck company (Dermasdat, Germany), and their solutions were prepared by dissolving their appropriate amount in double distilled water. MO (85%) and SY (90%) were purchased from Sigma-Aldrich company (USA). The pH was adjusted and measured using pH/ion meter model 686 (Metrohm, Switzerland). MO and SY concentration was determined using Jasco UV–Vis spectrophotometer model V-530 (Jasco, Japan). ZnS:Cu–NPs–AC were characterized by SEM (SEM: KYKY-EM3200, Hitachi company, China) under an acceleration voltage of 26 kV) and XRD (PW 1800, Philips, Germany). An ultrasonic bath (Tecno-GAZ SPA Ultrasonic System, Parma, Italy) at 40 kHz of frequency and 130 W of power was used for ultrasound-assisted adsorption procedure. Other chemicals and equipment were used according to previous publication [16–18,29].

2.2. Preparation of ZnS:Cu–NPs–AC

As synthesis of ZnS–NPs, 0.3 mmol of zinc acetate solution was mixed with 30 mL of 0.25 M thiourea solution and diluted with deionized water to 125 mL at pH = 6.0. Then, the solution was dispersed in ultrasonic bath for 1 h; subsequently, 0.5 mL of 0.2 M ($Cu(CH_3COO)_2$) solution was added to above solution, along with dispersion for 15 min, and color of solution slightly changes from milky white to light green because of the Cu^{2+} ions diffusion to ZnS and formation of ZnS:Cu–NPs suspension. Then, the mixture of the precursor solution was transferred to an autoclave at 100°C for 6 h. Finally, the obtained ZnS:Cu–NPs were filtered and washed several times by deionized water and dried at 80°C for 12 h. Finally, for deposition of ZnS:Cu–NPs on AC, 0.2 g of ZnS:Cu–NPs was dispersed in 30 mL ethanol so that in parallel 2.0 g AC was dispersed in 120 mL ethanol, after 30 min two solution was added together to the obtained ZnS:Cu–NPs–AC suspension and strong stirring for 20 h at room temperature. The prepared ZnS:Cu–NPs–AC were filtered, washed with ethanol and deionized water, and dried at 80°C for 12 h.

2.3. Combination of ultrasonication and adsorption processes

Ultrasonic assistant adsorption of MO and SY onto ZnS:Cu–NPs–AC was carried out as follows: 50 mL of

certain concentration of dyes solution at pH 5.0 was mixed thoroughly with certain amount of ZnS:Cu–NPs–AC in Erlenmeyer flask in an ultrasonic bath for 4 min at room temperature. Finally, the mixture was centrifuged, and the spectrum of dyes in the effluent solutions was recorded by UV–Vis spectrophotometer. Then, removal percentage of dyes (R%) and adsorption capacity of ZnS:Cu–NPs–AC (Q_e) was calculated according to our previous reports [30–32].

The absorption spectrum of MO and SY before and after the removal on the initial concentration of 10 and 20 mg L^{-1} and sonication time 4 min of the different adsorbent dosage (12–24 and 16–33 mg) showed in Figs. 2(a) and (b), respectively. As seen, each of MO and SY absorption spectra shows that maxima absorbance at wavelength of 465 and 427 nm, respectively, which their sensitivity significantly decreased following increasing adsorbent mass for two dyes. Accordingly, the wavelength of 465 and 427 nm was chosen as a sensitive wavelength for other analytical measurements of MO and SY.

2.4. Experimental design

CCD (using STATISTICA software version 10) was applied for optimization with least number of experiments through cheap and reduced amount of material and time via effective way. The CCD permits estimation of interaction among parameters in addition to their main effects. In CCD, numeric factors were varied over five levels including two levels for star or axial points (±α), two levels for factorial points or high/low levels (±1) and one level for center point following the undertaken 23 runs. The variable levels and design matrix and responses based on three variables of initial MO or SY concentration (x_1), adsorbent mass (x_2) and sonication time (x_3) on the removal percentage of MO or SY were tabulated in Table 1. The models was expressed by comparing the experimental and model predicted responses using normal probability plot of the studentized residuals to check its normality. A second-order polynomial equation permits modeling and further fitting and evaluation of data over well learning orthogonal space.

The analysis of variance (ANOVA) based on multiple correlation coefficients (the adjusted and predicted R^2) values gives unique worth welding knowledge about interaction of variables to obtain best operating conditions over three-dimensional (3D) response surface plots [33]. Also, desirability function (DF) gives information about the optimized condition and quality and acceptance of the process to understand and use [34,35].

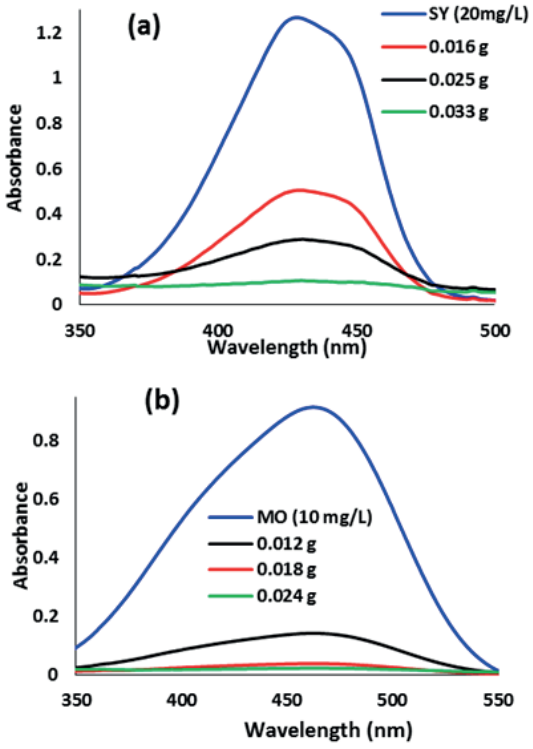

Fig. 2. Absorbance spectra of MO (a) and SY (b) after addition of different amount of ZnS:Cu–NPs–AC.

3. Results and discussion

3.1. Characterization of ZnS:Cu–NP–AC

The XRD patterns of the ZnS:Cu nanoparticles loaded AC (Fig. 3(a)) revealed three peaks at 28.9°, 48.05°, and 56.5° correspond to the (111), (220), and (311) lattice planes, respectively, which shown cubic zinc blende structure of ZnS (JCPDS No. 05-0566). Also, observed a peak at 54° is corresponded to the Cu purity and characteristic peaks of copper impurity (such as CuS, CuO) were not detected. In addition, a broad peak at 23.2° (002) is corresponded to the interlayer spacing of the AC. From the XRD pattern, the broadening of the diffraction peaks of the samples is obvious which materials are nanosized [36].

The morphology of ZnS:Cu–NPs–AC was studied by SEM (Figs. 3(b) and (c)), which shows spherical structure of ZnS:Cu–NPs with high surface area that showed good distribution over the surface of AC and could increase effective surface for adsorption of dyes under study.

3.2. Effect of pH

Chemical structures of MO and SY dyes show that their ionic charges in addition to ZnS:Cu NPs–AC nature are greatly affected by pH. The dyes adsorption occurs by combination of various mechanisms like ion exchange, hydrogen bonding, electrostatic, and soft–soft and dipole–ion interactions. Effects of shear force and solution pH on dyes under study adsorption over ZnS:Cu–NPs–AC surface were investigated in the range of 2–8 (Fig. 4). It was seen that in acidic pH simultaneous probable protonation of dyes and adsorbent lead to further repulsive force that extensively reduces the amount of removal percentage. Another main difficulty at such region is protonation of ZnS:Cu and its subsequent back distribution to initial aqueous solution that leads to strong reduction in removal percentages. At pH 5, dyes deprotonation leads to enhance their mass transfer and subsequent adsorption efficiency.

Table 1
Factors and levels, CCD experiments and the responses obtained

	Factorsww	Levels for MG				
		$-\alpha$	Low (–1)	Central (0)	High (+1)	$+\alpha$
x_1	Concentration of MG (mg L^{-1})	6.6	8	10	12	13.6
x_1	Adsorbent mass (g)	0.01	0.015	0.17	0.022	0.025
x_3	Sonication time (min)	3	3.4	4	4.6	5
x_1	Concentration of SY (mg L^{-1})	10	14	20	26	30
x_1	Adsorbent mass (g)	0.015	0.02	0.25	0.03	0.035
x_3	Sonication time (min)	3	3.4	4	4.6	5

Run	x_1	x_2	x_3	$R\%_{MO}$	x_1	x_2	x_3	$R\%_{SY}$
1	13.36	0.02	4.00	92.01	14.00	0.03	4.60	86.39
2	8.00	0.01	3.40	94.81	20.00	0.02	4.00	65.2
3	10.00	0.02	4.00	94.78	14.00	0.03	3.40	88.16
4	8.00	0.02	3.40	98.13	26.00	0.02	3.40	59.15
5	12.00	0.02	4.60	98.62	14.00	0.02	3.40	81.2
6	10.00	0.02	4.00	95.01	20.00	0.03	4.00	78.56
7	10.00	0.02	4.00	94.93	20.00	0.03	2.99	81.29
8	10.00	0.02	4.00	95.91	14.00	0.02	4.60	81.45
9	6.64	0.02	4.00	97.71	20.00	0.03	5.01	83.87
10	10.00	0.01	4.00	84.96	20.00	0.03	4.00	78.64
11	8.00	0.01	4.60	95.7	30.09	0.03	4.00	62.67
12	10.00	0.02	2.99	95.35	20.00	0.03	4.00	80.36
13	10.00	0.02	4.00	97.78	9.91	0.03	4.00	87.69
14	8.00	0.02	4.60	98.19	20.00	0.03	4.00	87.69
15	10.00	0.02	4.00	95.13	26.00	0.02	4.60	62.32
16	10.00	0.02	4.00	95.56	20.00	0.03	4.00	80.1
17	12.00	0.01	3.40	86.18	20.00	0.03	4.00	78.4
18	12.00	0.02	3.40	96.53	26.00	0.03	4.60	82.27
19	12.00	0.01	4.60	87.7	26.00	0.03	3.40	79.16
20	10.00	0.02	4.00	94.9	20.00	0.03	4.00	79.85
21	10.00	0.02	5.01	98.6	20.00	0.03	4.00	81.76
22	13.36	0.02	4.00	92.01	14.00	0.03	4.60	86.39
23	8.00	0.01	3.40	94.81	20.00	0.02	4.00	65.2

At pH higher than 6, probable competition of hydroxide with dyes and also formation of similar negative charge on dyes and adsorbent cause significant decrease in dyes removal percentage. Both at high acidic and basic media, expected unstability of ZnS:Cu–NPs leads to reduce the dyes removal percentage and subsequently lower the lifetime and reusability of adsorbent. Therefore, all subsequent adsorption experiments were conducted at pH 5.0, which has maximum adsorption efficiency.

3.3. CCD analysis

The ANOVA related to full quadratic model for $R\%_{MO}$ and $R\%_{SY}$ (see Table 2) has good F values (109.36 and 151.94) and p values (<0.0001 and <0.0001) with a lack of fit p value of 0.1214 and 0.8502, respectively. The lack of fit p value for $R\%_{MO}$ and $R\%_{SY}$ show its ignorable part toward pure error that imply the model suitability for fitting real behavior of under study adsorption. However, the p values corresponding to the terms of x_1, x_2, x_3, x_1x_2, x_2^2 and x_3^2 and x_1, x_2, x_3, x_1x_2, x_1x_3, x_1^2, x_2^2 and x_3^2 for $R\%_{MO}$ and $R\%_{SY}$, respectively, are less than 0.05 that suggest their significant contribution in response. Therefore, the following response, surface quadratic model, was finally applied for prediction of $R\%_{MO}$ and $R\%_{SY}$:

$$R\%_{MO} = 133.0328 - 6.7964x_1 + 2300.5139x_2 - 16.0031x_3 + 276.0714x_1x_2 - 1.07614E + 005x_2^2 + 1.8427x_3^2 \quad (1)$$

$$R\%_{SY} = 129.30 - 3.31294x_1 + 1792.3308x_2 - 22.8894x_3 + 116.9166x_1x_2 + 0.2708x_1x_3 - 0.0467x_1^2 - 0.49412x_2^2 + 2.5937x_3^2 \quad (2)$$

The values of the determination coefficient R^2 (0.9889 and 0.9920), predicated R^2 (0.9355 and 0.9768) and the adjusted R^2 (0.9799 and 0.9855) for $R\%_{MO}$ and $R\%_{SY}$, respectively, in addition to low and acceptable standard deviation values, low PRESS value, low coefficient of variation, and low standard error for model (Table 3) indicate that the response surface quadratic models are the appropriate for the best prediction of MO and SY removal efficiency. The adequate precision ratio of these models for $R\%_{MO}$ and $R\%_{SY}$ were found to be 35.396 and 41.651 that indicates the sufficiency of models for MO and SY removal.

3.4. Desirability function combined with CCD

The best condition for the achievement of maximum response was used and tested by STATISTICA 10.0

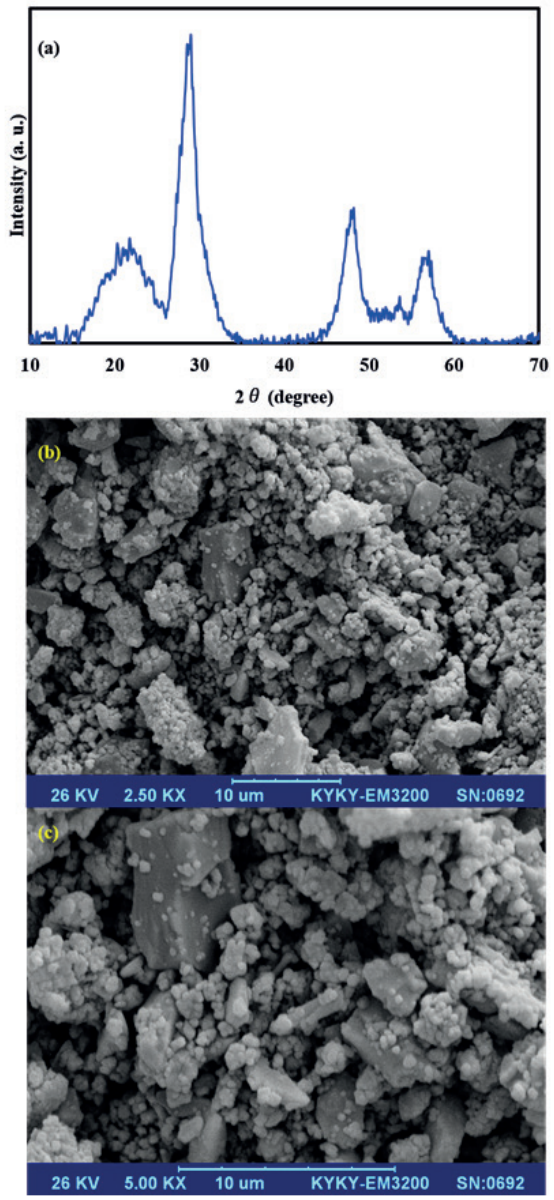

Fig. 3. XRD pattern (a) and SEM image in two magnifications (b and c) of the prepared ZnS:Cu–NPs–AC.

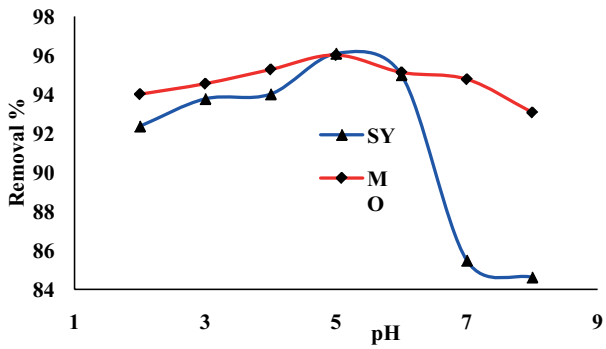

Fig. 4. Effect of pH on removal of MO and SY dyes.

software (Fig. 5); in this method, desirability values of the minimum, middle and maximum were configured as 0.0, 0.5 and 1.0, respectively. The desirability of 1.0 and closer value is an indication of optimum operating conditions. Left-hand side of DFs plot shows *R*% of MO and SY, while level, bottom side shows change of each variables and right-hand side of these profiles shows the application of individual desirability numerals calculation of the $R\%_{MO}$ and $R\%_{SY}$. The desirability scores of 0.9086 and 0.9441 show maximum removal percentage of 97.37% and 86.54% for MO and SY, respectively. These maximum removal percentages are obtained at the following best operational 6.64 and 12 mg L^{-1} of MO and SY, 0.018 and 0.029 g of ZnS:Cu–NP–AC and 4.0 and 4.5 min of sonication time for *R*% of MO and SY, respectively.

3.5. 3D surface plots

3D surface plots (Fig. 6) were obtained for a given pair of actual factors at fixed and central values of other variables.

The effects of adsorbent dosage on the MO and SY removal percentage (Figs. 6(a) and (b)) show that lower adsorbent dosage leads to diminish in dyes adsorption because of the unbalanced dye molecules to vacant sites of ZnS:Cu–NP–AC. The greater specific surface area and availability of more adsorption sites that obtained at either higher adsorbent mass or lower dyes concentration cause strong enhanced removal percentage (Figs. 6(a)–(c)). The opposite correlation at higher dyes concentrations is occurred due to the saturation of adsorption sites. These results indicate that MO and SY accumulation onto ZnS:Cu–NPs–AC immensity depends on their initial concentration.

The effect of sonication time on the SY percentage removal is presented in Fig. 6(c). As seen, the maximum adsorption of SY at short sonication time suggests high contribution of ultrasound power in mass transfer and simultaneously increases available surface area and vacant sites of adsorbent. The mass transfer increase is due to raising diffusion coefficient encounter. These figures also show occurrence of more than 95% of MO and SY in the first 3 min, while 4 min sonication is sufficient to reach equilibrium.

3.6. Adsorption kinetics

Adsorption kinetics is an important characteristic in studying adsorption process to explore their complex kinetics. Various kinetic models like pseudo-first-order and pseudo-second-order models, Elovich equation and intraparticle diffusion model (Table 4) were tested to describe the MO and SY adsorption process onto ZnS:Cu–NP–AC [15,37,38]. Each of the investigated models was fitted by a linear regression to the experimental data, evaluating their appropriateness on the basis of the corresponding determination coefficients (R^2). The rate constants of best model were applied for the estimation of the activation parameters. The agreement of experimental data and the model-predicted values was expressed by the correlation and determination coefficients (R^2, values close agreement between experimental and equilibrium adsorption capacity). R^2 values for pseudo-second-order kinetic model are high (~1) for latter,

Table 2
ANOVA for the quadratic model applied for removal of MO and SY

Source of variation	DF[a]	$R\%_{MO}$				$R\%_{SY}$			
		SS[b]	MS[c]	*F* value	*p* value	SS	MS	*F* value	*p* value
Model	9	300.77	33.42	109.36	<0.0001	1461.92	162.44	151.94	<0.0001
x_1	1	54.92	54.92	179.72	<0.0001	680.16	680.16	636.19	<0.0001
x_2	1	173.24	173.24	566.92	<0.0001	588.94	588.94	550.87	<0.0001
x_3	1	7.36	7.36	24.09	0.0005	6.06	6.06	5.67	0.0364
x_1x_2	1	29.88	29.88	97.77	<0.0001	98.42	98.42	92.06	<0.0001
x_1x_3	1	0.88	0.88	2.89	0.1170	7.61	7.61	7.11	0.0219
x_2x_3	1	8.450E-003	8.450E-003	0.028	0.8709	0.54	0.54	0.51	0.4918
x_1^2	1	0.11	0.11	0.35	0.5663	42.49	42.49	39.74	<0.0001
x_2^2	1	26.08	26.08	85.36	<0.0001	22.90	22.90	21.42	0.0007
x_3^2	1	6.61	6.61	21.62	0.0007	13.09	13.09	12.24	0.0050
Residual	11	3.36	0.31			11.76	1.07		
Lack of fit	5	2.35	0.47	2.80	0.1214	2.79	0.56	0.37	0.8502
Pure error	6	1.01	0.17			8.97	1.49		
Cor. total	20	304.13	33.42			1,473.68	162.44		

[a]Degrees of freedom.
[b]Sum of squares.
[c]Mean square.

Table 3
Quadratic model summary statistics and quality for removal of MO and SY

Statistics quality of model	$R\%_{MO}$	$R\%_{SY}$
Standard deviation	0.55	1.03
Mean	94.69	78.38
Coefficient variation, %	0.58	1.32
PRESS	19.62	34.14
R^2	0.9889	0.9920
Adjust R^2	0.9799	0.9855
Predicated R^2	0.9355	0.9768
Adequate precision ratio	35.396	41.651

and the calculated q_e values are mainly close to the experimental data. These two outcomes are criterion for judgment about applicability of each model for best prediction of adsorption data.

3.7. Adsorption equilibrium

Ultrasonic adsorption isotherm studies are being used to design efficient adsorption systems to explain the equilibrium relationship between equilibrium dye concentrations. The equilibrium adsorption of MO or SY (q_e vs. C_e) onto ZnS:Cu–NP–AC at some different adsorbent mass was undertaken to achieve conditions for application in waste water treatment. The equilibrium trend related to SY or MO adsorption was fitted to Langmuir, Freundlich, Temkin and Dubinin–Radushkevich isotherms (Table 5). It was found that R^2 value of Langmuir is about 1.0 that suggests the favorable

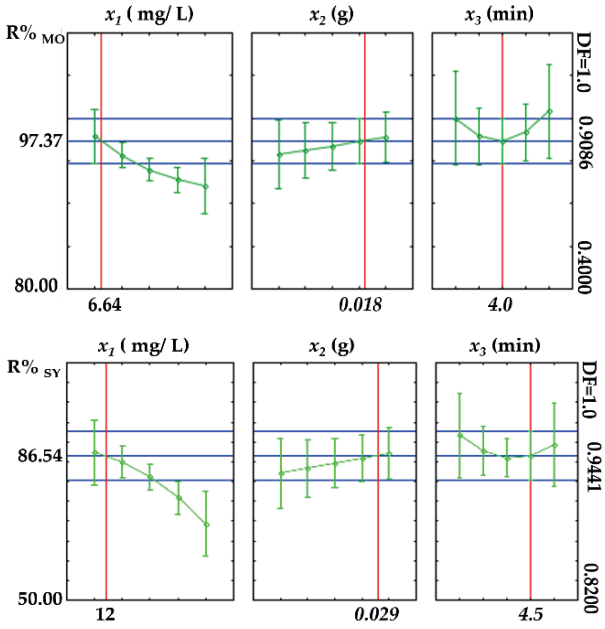

Fig. 5. DF profile for removal of MO and SY.

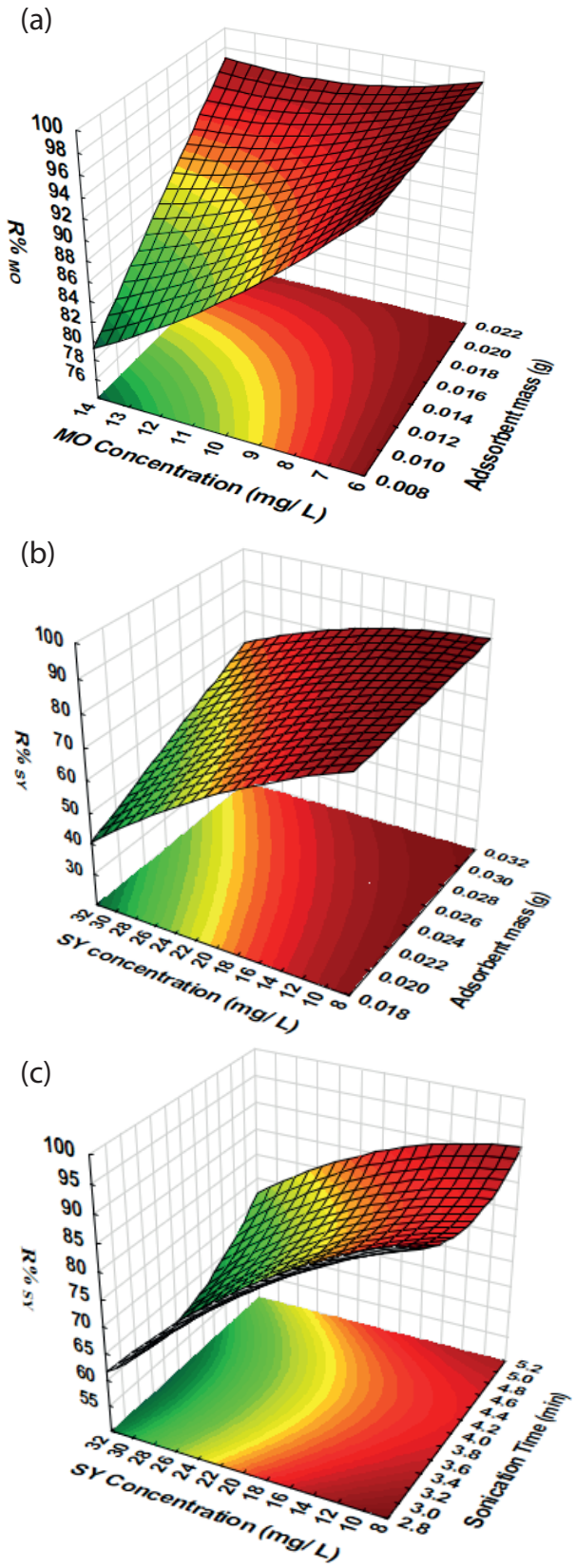

Fig. 6. Response surface plots: (a) MO concentration against adsorbent mass, (b) SY concentration against adsorbent mass and (c) SY concentration against sonication time.

adsorption explain. On the other hand, increase in K_L value with rising initial MO and SY concentration and adsorbent dosage shows high tendency of MO and SY for adsorption onto ZnS:Cu–NP–AC.

3.8. Thermodynamic study

Thermodynamic parameters provide additional information concerning internal energy change during dyes absorption onto ZnS:Cu–NP–AC are investigated (see Table 6). The parameters of free energy change ($\Delta G°$), enthalpy change ($\Delta°$) and entropy ($\Delta S°$) for the adsorption of dyes were calculated using the following equations:

$$\Delta G^{\circ} = -RT\mathrm{Ln}K_0 \tag{3}$$

$$\Delta S^{\circ} = \Delta H^{\circ} - \Delta G^{\circ}\mathrm{T} \tag{4}$$

where R is the universal gas constant (8.314 J mol^{-1} K^{-1}); T is the absolute temperature (K) and K_0 the thermodynamic equilibrium constant (values of K_0 may be calculated from the relation $\ln(q_e/C_e)$ vs. q_e at different temperatures and extrapolating to zero). The negative $\Delta G°$ values confirm the spontaneous nature and feasibility of the adsorption process. The $\Delta G°$ values were decreased as the temperature was elevated from 300.15 to 328.15 K, which is an indication of the physical adsorption nature of the process. The values of other parameters such as enthalpy change ($\Delta H°$) and entropy change ($\Delta S°$) may be determined from Van't Hoff equation:

$$\mathrm{Ln}K = \frac{\Delta S^{\circ}}{R} - \frac{\Delta H^{\circ}}{RT} \tag{5}$$

$\Delta H°$ and $\Delta G°$ can be obtained from the slope and intercept of Van't Hoff plot of ln$K$ vs. $1/T$. The negative values of $\Delta H°$ further confirm the endothermic nature of the adsorption process, while the negative $\Delta S°$ values suggest the decrease in adsorbate concentration in solid–liquid interface indicating thereby the increase in adsorbate concentration onto the solid phase. To further support the assertion that physical adsorption is the predominant mechanism, the values of activation energy (E_a) and sticking probability (S^*) were estimated from the experimental data using modified Arrhenius-type equation related to surface coverage (h) as follows [39–41]:

$$S^{*} = (1-\theta)e^{\frac{-E_a}{RT}} \tag{6}$$

The sticking probability (S^*) is a function of the adsorbate/adsorbent system under investigation. The parameter S^* shows the measure of the potential of an adsorbate to remain on the adsorbent indefinite. The values of S^* for MO and SY were found to be 3.2×10^{-3} and 3.4×10^{-3}, respectively, that lies in the range $0 < S^* < 1$ and depends on the temperature of the

Table 4
Isotherm constant parameters and correlation coefficients calculated for the dyes adsorption onto ZnS:Cu–NPs–AC

Isotherm	Parameters	Value					
		SY			MO		
		0.003 g	0.033 g	0.036 g	0.015 g	0.002 g	0.025 g
Langmuir	Q_m (mg g^{-1})	50.5412	44.2562	41.3303	44.6508	37.0420	33.9035
	K_L (L mg^{-1})	0.5465	2.6583	3.0244	2.7994	5.3992	5.6722
	R^2	0.9649	0.9931	0.9961	0.9811	0.9992	0.9872
Freundlich	1/n	0.3198	0.2249	0.2226	0.187	0.2271	0.3072
	K_F (L mg^{-1})	3.8347	4.4906	4.4114	4.5626	4.4482	4.4171
	R^2	0.9086	0.9521	0.9906	0.8402	0.9946	0.9736
Temkin	B_1	10.676	7.6077	6.9482	6.5089	6.349	7.0169
	K_T (L mg^{-1})	6.3719	66.3947	82.8330	160.744	133.991	68.7810
	R^2	0.8941	0.9493	0.9827	0.8294	0.9946	0.9602
Dubinin–Radushkevich	Q_s (mg g^{-1})	39.2244	40.1250	36.6238	38.6984	33.8419	29.9670
	$B \times 10^{-7}$	–4	–0.7	–0.5	–0.4	–0.3	–0.2
	E	1,581.14	3,779.64	4,472.15	5,000	5,773.67	7,072.13
	R^2	0.7939	0.9576	0.9246	0.6881	0.9724	0.9362

Table 5
Kinetic parameters for the adsorption of dyes onto ZnS:Cu–NPs–AC

Model	Parameters	Value	
		MO (13 mg L^{-1}, 0.02 g)	SY (28 mg L^{-1}, 0.033 g)
Pseudo-first-order kinetic	k_1 (min^{-1})	0.6139	0.7470
	q_e (cal) (mg g^{-1})	7.1466	7.9909
	R^2	0.9739	0.8865
Pseudo-second-order kinetic	k_2 (min^{-1})	0.1528	0.1679
	q_e (cal) (mg g^{-1})	31.25	41.6667
	R^2	0.9995	0.9996
Intraparticle diffusion	K_{diff} (mg g^{-1} min$^{-1/2}$)	2.8351	2.5134
	C (mg g^{-1})	23.877	34.489
	R^2	0.997	0.9788
Elovich	β (g mg^{-1})	0.4616	0.5272
	α (mg g^{-1} min^{-1})	43.50	33.25
	R^2	0.9928	0.9506

system. The surface coverage (h) can be calculated from the following equation [41]:

$$\theta = 1 - \frac{C_e}{C_0} \tag{7}$$

The activation energy and sticking probability were estimated from a plot of ln(1–θ) vs. 1/T (Table 6).

3.9. Comparison of this adsorbent with literature

Comparison of performance of the proposed method and this adsorbent with other methods and some adsorbents is summarized in Table 7. Accordingly, the ZnS:Cu–NPs–AC is superior to all other applied adsorbent in term of satisfactory removal performance for MO and SY. The results indicated that the combination of ultrasound with ZnS:Cu–NPs–AC causes acceleration of mass transfer rate in less contact time (<4.5 min), as well as coupled metallic nanoparticles with AC cause the increase in the adsorption capacity [42–44].

4. Conclusion

In this work, ZnS:Cu–NPs–AC was synthesized and was successfully applied for ultrasound-assisted adsorption of MO or SY in single solution. Effect of operational parameter such as pH was optimized using one-at-a-time method, and the contribution of other experimental parameters was followed by CCD. The interaction and main effect of variables were estimated by ANOVA and 3D surface plots. The p values of the terms x_1, x_2, x_3, x_1x_2, x_2^2 and x_3^2 and x_1, x_2, x_3, x_1x_2, x_1x_3, x_1^2, x_2^2 and x_3^2 for $R\%_{MO}$ and $R\%_{SY}$, respectively, are less than 0.05 that suggest their significant contribution on each response. The isotherm equilibrium data were best described by the Langmuir model, while the kinetics and rate of adsorption at most situation were successfully fitted by pseudo-second-order model. The comparison of obtained results shows that ZnS:Cu–NPs–AC has better performance for SY toward MO. Finally, comparison with literature shows that the proposed method has revealed good potential in the efficient removal of these dyes from aqueous solution than to several other adsorbents and methods.

Table 6
Thermodynamic parameters for the adsorption of MO and SY onto ZnS:Cu–NPs–AC

Parameter	Temperature (K)				
	300.15	307.15	314.15	321.15	328.15
Methyl orange					
$\Delta G°$	–6,028.79	–7,675.44	–8,909.38	–9,966.99	–10,795.6
K_0	11.2	20.2	30.3	41.8	52.3
$\Delta H°$ kJ mol^{-1}	0.0016628				
$\Delta S°$ J mol^{-1} K^{-1}	0.0324246				
Ea	0.0015421				
*S**	3.2×10^{-3}				
Sunset yellow					
$\Delta G°$	–5,537.9	–6,846.38	–8,166.61	–9,134.21	–10,002.1
K_0	9.2	14.6	22.8	30.6	39.1
$\Delta H°$ kJ mol^{-1}	0.0016628				
$\Delta S°$ J mol^{-1} K^{-1}	0.0315932				
Ea	0.0016628				
*S**	3.4×10^{-3}				

Table 7
Comparison with some reported literatures

Adsorbent	Dye	Contact time (min)	Adsorption capacity (mg g^{-1})	Reference
Protonated cross-linked chitosan	MO	30	89	[45]
Multiwalled carbon nanotubes	MO	60	42–78	[46]
Carbon-coated monolith	MO	80	47–23	[47]
Ammonium-functionalized silica nanoparticle	MO	40	105	[13]
Au–NP–AC	MO	20	161	[48]
Tamarisk–AC	MO	45	3.84	[48]
ZnS:Cu–NPs–AC	MO	4.5	44.65	Our work
ZnS:Ni–NP–AC	SY	3.8	–	[42]
CuS–NP–AC	SY	17	122	[43]
$Zn(OH)_2$–NP–AC	SY	30	158.7	[44]
Ionic liquid based PMO	SY	2.0	208	[49]
NiS–NP–AC	SY	15	333.3	[50]
SnO_2–NP–AC	SY	20	7.89	[51]
ZnO–NPs–AC	SY	30	142.85	[52]
Au–NP–AC	SY	30	227.27	[53]
Wood activated carbon	SY	10	4.89	[54]
Orange activated carbon	SY	30	30.82	[54]
$Zn(OH)_2$–NP–AC	SY	5.2	83–114	[55]
ZnS:Cu–NPs–AC	MO	4.5	50.54	Our work

Acknowledgments

The authors would like to thank the Research Council of the Yasouj University for financial support to this work.

References

[1] P. Sharma, M.R. Das, Removal of a cationic dye from aqueous solution using graphene oxide nanosheets: investigation of adsorption parameters, J. Chem. Eng. Data, 58 (2012) 151–158.
[2] X. Zhu, Y. Liu, C. Zhou, S. Zhang, J. Chen, Novel and high-performance magnetic carbon composite prepared from waste hydrochar for dye removal, ACS Sustain. Chem. Eng., 2 (2014) 969–977.
[3] M. Ghaedi, M.R. Rahimi, A.M. Ghaedi, I. Tyagi, S. Agarwal, V.K. Gupta, Application of least squares support vector regression and linear multiple regression for modeling removal of methyl orange onto tin oxide nanoparticles loaded on activated carbon and activated carbon prepared from *Pistacia atlantica* wood, J. Colloid Interface Sci., 461 (2016) 425–434.
[4] N.H. Azmi, U.F.M. Ali, F. Muhammad Ridwan, K.M. Isa, N.Z. Zulkurnai, M.K. Aroua, Preparation of activated carbon using sea mango (Cerbera odollam) with microwave-assisted technique for the removal of methyl orange from textile wastewater, Desal. Wat. Treat., 57 (2016) 29143–29152.
[5] Y. Zhang, J. Li, W. Li, G. Chen, Utilization of inactivated aerobic granular sludge as a potential adsorbent for the removal of sunset yellow FCF, Desal. Wat. Treat., 57 (2016) 7334–7344.
[6] K.I. Hussain, M. Usman, M. Siddiq, N. Rasool, M.F. Nazar, I. Ahmad, A.A. Holder, A.A. Altaf, Application of micellar enhanced ultra-filtration for the removal of sunset yellow dye from aqueous media, J. Dispers. Sci. Technol. 38 (2017) 139–144.
[7] A.K. Verma, R.R. Dash, P. Bhunia, A review on chemical coagulation/flocculation technologies for removal of colour from textile wastewaters, J. Environ. Manage., 93 (2012) 154–168.
[8] M. Asgher, H.N. Bhatti, Evaluation of thermodynamics and effect of chemical treatments on sorption potential of *Citrus* waste biomass for removal of anionic dyes from aqueous solutions, Ecol. Eng., 38 (2012) 79–85.
[9] B.K. Körbahti, K. Artut, C. Geçgel, A. Özer, Electrochemical decolorization of textile dyes and removal of metal ions from textile dye and metal ion binary mixtures, Chem. Eng. J., 173 (2011) 677–688.
[10] V. Gupta, Application of low-cost adsorbents for dye removal–a review, J. Environ. Manage., 90 (2009) 2313–2342.
[11] E. Oguz, B. Keskinler, Z. Çelik, Ozonation of aqueous Bomaplex Red CR-L dye in a semi-batch reactor, Dyes Pigm., 64 (2005) 101–108.
[12] A. Duran, M. Tuzen, M. Soylak, Preconcentration of some trace elements via using multiwalled carbon nanotubes as solid phase extraction adsorbent, J. Hazard. Mater., 169 (2009) 466–471.
[13] M. Tuzen, K.O. Saygi, C. Usta, M. Soylak, *Pseudomonas aeruginosa* immobilized multiwalled carbon nanotubes as biosorbent for heavy metal ions, Bioresour. Technol., 99 (2008) 1563–1570.
[14] M. Tuzen, K.O. Saygi, M. Soylak, Solid phase extraction of heavy metal ions in environmental samples on multiwalled carbon nanotubes, J. Hazard. Mater., 152 (2008) 632–639.
[15] M. Ghaedi, A. Hassanzadeh, S.N. Kokhdan, Multiwalled carbon nanotubes as adsorbents for the kinetic and equilibrium study of the removal of alizarin red S and morin, J. Chem. Eng. Data, 56 (2011) 2511–2520.
[16] C. Namasivayam, D. Kavitha, Removal of Congo Red from water by adsorption onto activated carbon prepared from coir pith, an agricultural solid waste, Dyes Pigm., 54 (2002) 47–58.
[17] V. Gupta, B. Gupta, A. Rastogi, S. Agarwal, A. Nayak, Pesticides removal from waste water by activated carbon prepared from waste rubber tire, Water Res., 45 (2011) 4047–4055.
[18] M. Gonçalves, M.C. Guerreiro, L.C.A. de Oliveira, C.S. de Castro, A friendly environmental material: iron oxide dispersed over activated carbon from coffee husk for organic pollutants removal, J. Environ. Manage., 127 (2013) 206–211.
[19] A. Hassani, R.D.C. Soltani, M. Kıranşan, S. Karaca, C. Karaca, A. Khataee, Ultrasound-assisted adsorption of textile dyes using modified nanoclay: central composite design optimization, Korean J. Chem. Eng., 33 (2016) 178–188.
[20] A. Khataee, B. Kayan, D. Kalderis, A. Karimi, S. Akay, M. Konsolakis, Ultrasound-assisted removal of Acid Red 17 using nanosized Fe_3O_4-loaded coffee waste hydrochar, Ultrason. Sonochem., 35 (2016) 72–80.
[21] A. Asfaram, M. Ghaedi, K. Dashtian, Ultrasound assisted combined molecularly imprinted polymer for selective extraction of nicotinamide in human urine and milk samples: spectrophotometric determination and optimization study, Ultrason. Sonochem., 34 (2017) 640–650.
[22] S. Mosleh, M.R. Rahimi, M. Ghaedi, K. Dashtian, Sonophotocatalytic degradation of trypan blue and vesuvine dyes in the presence of blue light active photocatalyst of Ag_3PO_4/Bi_2S_3-HKUST-1-MOF: central composite optimization and synergistic effect study, Ultrason. Sonochem., 32 (2016) 387–397.
[23] F.N. Azad, M. Ghaedi, K. Dashtian, S. Hajati, V. Pezeshkpour, Ultrasonically assisted hydrothermal synthesis of activated carbon–HKUST-1-MOF hybrid for efficient simultaneous ultrasound-assisted removal of ternary organic dyes and antibacterial investigation: Taguchi optimization, Ultrason. Sonochem., 31 (2016) 383–393.
[24] F.N. Azad, M. Ghaedi, K. Dashtian, A. Jamshidi, G. Hassani, M. Montazerozohori, S. Hajati, M. Rajabi, A.A. Bazrafshan, Preparation and characterization of an AC–Fe_3O_4–Au hybrid for the simultaneous removal of Cd^{2+}, Pb^{2+}, Cr^{3+} and Ni^{2+} ions from aqueous solution via complexation with 2-((2, 4-dichloro-benzylidene)-amino)-benzenethiol:Taguchi optimization, RSC Adv., 6 (2016) 19780–19791.
[25] M. Ghaedi, F.N. Azad, K. Dashtian, S. Hajati, A. Goudarzi, M. Soylak, Central composite design and genetic algorithm applied for the optimization of ultrasonic-assisted removal of malachite green by ZnO nanorod-loaded activated carbon, Spectrochim. Acta, Part A, 167 (2016) 157–164.
[26] M. Jamshidi, M. Ghaedi, K. Dashtian, S. Hajati, A.A. Bazrafshan, Sonochemical assisted hydrothermal synthesis of ZnO:Cr nanoparticles loaded activated carbon for simultaneous ultrasound-assisted adsorption of ternary toxic organic dye: derivative spectrophotometric, optimization, kinetic and isotherm study, Ultrason. Sonochem., 32 (2016) 119–131.
[27] A. Asfaram, M. Ghaedi, K. Dashtian, Rapid ultrasound-assisted magnetic microextraction of gallic acid from urine, plasma and water samples by HKUST-1-MOF-Fe_3O_4-GA-MIP-NPs: UV–vis detection and optimization study, Ultrason. Sonochem., 34 (2017) 561–570.
[28] S. Mosleh, M.R. Rahimi, M. Ghaedi, K. Dashtian, S. Hajati, $BiPO_4$/Bi_2S_3-HKUST-1-MOF as a novel blue light-driven photocatalyst for simultaneous degradation of toluidine blue and auramine-O dyes in a new rotating packed bed reactor: optimization and comparison to a conventional reactor, RSC Adv., 6 (2016) 63667–63680.
[29] M. Ghaedi, H.A. Larki, S.N. Kokhdan, F. Marahel, R. Sahraei, A. Daneshfar, M. Purkait, Synthesis and characterization of zinc sulfide nanoparticles loaded on activated carbon for the removal of methylene blue, Environ. Prog. Sustain. Energy, 32 (2013) 535–542.
[30] M. Ghaedi, A. Ansari, M. Habibi, A. Asghari, Removal of malachite green from aqueous solution by zinc oxide nanoparticle loaded on activated carbon: kinetics and isotherm study, J. Ind. Eng. Chem., 20 (2014) 17–28.
[31] M. Ghaedi, M. Pakniat, Z. Mahmoudi, S. Hajati, R. Sahraei, A. Daneshfar, Synthesis of nickel sulfide nanoparticles loaded on activated carbon as a novel adsorbent for the competitive removal of Methylene blue and Safranin-O, Spectrochim. Acta, Part A, 123 (2014) 402–409.
[32] M. Ghaedi, H. Tavallali, M. Sharifi, S.N. Kokhdan, A. Asghari, Preparation of low cost activated carbon from Myrtus communis and pomegranate and their efficient application for removal of Congo red from aqueous solution, Spectrochim. Acta, Part A, 86 (2012) 107–114.

[33] V. Stanić, S. Dimitrijević, D.G. Antonović, B.M. Jokić, S.P. Zec, S.T. Tanasković, S. Raičević, Synthesis of fluorine substituted hydroxyapatite nanopowders and application of the central composite design for determination of its antimicrobial effects, Appl. Surf. Sci., 290 (2014) 346–352.
[34] K. Yetilmezsoy, S.A. Abdul-Wahab, A composite desirability function-based modeling approach in predicting mass condensate flux of condenser in seawater greenhouse, Desalination, 344 (2014) 171–180.
[35] S. Khodadoust, M. Hadjmohammadi, Determination of N-methylcarbamate insecticides in water samples using dispersive liquid–liquid microextraction and HPLC with the aid of experimental design and desirability function, Anal. Chim. Acta, 699 (2011) 113–119.
[36] A. Goudarzi, G.M. Aval, R. Sahraei, H. Ahmadpoor, Ammonia-free chemical bath deposition of nanocrystalline ZnS thin film buffer layer for solar cells, Thin Solid Films, 516 (2008) 4953–4957.
[37] A.B. Albadarin, C. Mangwandi, H. Ala'a, G.M. Walker, S.J. Allen, M.N. Ahmad, Kinetic and thermodynamics of chromium ions adsorption onto low-cost dolomite adsorbent, Chem. Eng. J., 179 (2012) 193–202.
[38] M. Ghaedi, Z. Andikaey, A. Daneshfar, T. Akbari, R. Sahraei, Removal of Acid Red 299 dye on gold nanoparticles loaded on activated carbon: kinetic and thermodynamic investigation of the removal process, Desal. Wat. Treat., 52 (2014) 5494–5503.
[39] M.R. Ganjali, A. Rouhollahi, A.R. Mardan, M. Shamsipur, Thermodynamic study of the binding of hexathia-18-crown-6-tetraone with some transition and heavy metal ions in dimethyl sulfoxide solution, J. Chem. Soc., Faraday Trans., 94 (1998) 1959–1962.
[40] M. Ghaedi, B. Sadeghian, A.A. Pebdani, R. Sahraei, A. Daneshfar, C. Duran, Kinetics, thermodynamics and equilibrium evaluation of direct yellow 12 removal by adsorption onto silver nanoparticles loaded activated carbon, Chem. Eng. J., 187 (2012) 133–141.
[41] M. Ghaedi, A. Shokrollahi, H. Hossainian, S.N. Kokhdan, Comparison of activated carbon and multiwalled carbon nanotubes for efficient removal of eriochrome cyanine R (ECR): kinetic, isotherm, and thermodynamic study of the removal process, J. Chem. Eng. Data, 56 (2011) 3227–3235.
[42] M. Roosta, M. Ghaedi, A. Daneshfar, S. Darafarin, R. Sahraei, M. Purkait, Simultaneous ultrasound-assisted removal of sunset yellow and erythrosine by ZnS:Ni nanoparticles loaded on activated carbon: optimization by central composite design, Ultrason. Sonochem., 21 (2014) 1441–1450.
[43] S. Khodadoust, M. Ghaedi, R. Sahraei, A. Daneshfar, Application of experimental design for removal of sunset yellow by copper sulfide nanoparticles loaded on activated carbon, J. Ind. Eng. Chem., 20 (2014) 2663–2670.
[44] M. Ghaedi, A.M. Ghaedi, E. Negintaji, A. Ansari, F. Mohammadi, Artificial neural network – imperialist competitive algorithm based optimization for removal of sunset yellow using $Zn(OH)_2$ nanoparticles-activated carbon, J. Ind. Eng. Chem., 20 (2014) 4332–4343.
[45] B.K. Suyamboo, R. Perumal, Equilibrium, thermodynamic and kinetic studies on adsorption of a basic dye by *Citrullus lanatus* rind, Iran. J. Energy Environ., 3 (2012) 23–34.
[46] F. Taghizadeh, M. Ghaedi, K. Kamali, E. Sharifpour, R. Sahraie, M. Purkait, Comparison of nickel and/or zinc selenide nanoparticle loaded on activated carbon as efficient adsorbents for kinetic and equilibrium study of removal of Arsenazo (III) dye, Powder Technol., 245 (2013) 217–226.
[47] M. Temkin, V. Pyzhev, Kinetics of ammonia synthesis on promoted iron catalysts, Acta Physiochim. URSS, 12 (1940) 217–222.
[48] M. Ghaedi, A. Ghaedi, A. Ansari, F. Mohammadi, A. Vafaei, Artificial neural network and particle swarm optimization for removal of methyl orange by gold nanoparticles loaded on activated carbon and tamarisk, Spectrochim. Acta, Part A, 132 (2014) 639–654.
[49] M. Ghaedi, D. Elhamifar, M. Roosta, R. Moshkelgosha, Ionic liquid based periodic mesoporous organosilica: an efficient support for removal of sunset yellow from aqueous solutions under ultrasonic conditions, J. Ind. Eng. Chem., 20 (2014) 1703–1712.
[50] M. Ghaedi, N. Zeinali, M. Maghsoudi, M. Purkait, Artificial neural network (ANN) method for modeling of sunset yellow dye adsorption using nickel sulfide nanoparticle loaded on activated carbon: kinetic and isotherm study, J. Dispers. Sci. Technol., 36 (2015) 1339–1348.
[51] S. Hajati, M. Ghaedi, Z. Mahmoudi, R. Sahraei, SnO_2 nanoparticle-loaded activated carbon for simultaneous removal of Acid Yellow 41 and Sunset Yellow; derivative spectrophotometric, artificial neural network and optimization approach, Spectrochim. Acta, Part A, 150 (2015) 1002–1012.
[52] M. Maghsoudi, M. Ghaedi, A. Zinali, A.M. Ghaedi, M.H. Habibi, Artificial neural network (ANN) method for modeling of sunset yellow dye adsorption using zinc oxide nanorods loaded on activated carbon: kinetic and isotherm study, Spectrochim. Acta, Part A, 134 (2015) 1–9.
[53] M. Ghaedi, F. Mohammdi, A. Ansari, Gold nanoparticles loaded on activated carbon as novel adsorbent for kinetic and isotherm studies of methyl orange and sunset yellow adsorption, J. Dispers. Sci. Technol., 36 (2015) 652–659.
[54] A. Ghaedi, M. Ghaedi, P. Karami, Comparison of ultrasonic with stirrer performance for removal of sunset yellow (SY) by activated carbon prepared from wood of orange tree: artificial neural network modeling, Spectrochim. Acta, Part A, 138 (2015) 789–799.
[55] M. Roosta, M. Ghaedi, R. Sahraei, M.K. Purkait, Ultrasonic assisted removal of sunset yellow from aqueous solution by zinc hydroxide nanoparticle loaded activated carbon: optimized experimental design, Mater. Sci. Eng., C, 52 (2015) 82–89.